

# Compton polarimeter as a focal plane detector for hard X-ray telescope: sensitivity estimation with Geant4 simulations

T. Chattopadhyay · S. V. Vadawale · J. Pendharkar

Received: 21 May 2012 / Accepted: 27 July 2012 / Published online: 12 September 2012  
© Springer Science+Business Media B.V. 2012

**Abstract** X-ray polarimetry can be an important tool for investigating various physical processes as well as their geometries at the celestial X-ray sources. However, X-ray polarimetry has not progressed much compared to the spectroscopy, timing and imaging mainly due to the extremely photon-hungry nature of X-ray polarimetry leading to severely limited sensitivity of X-ray polarimeters. The great improvement in sensitivity in spectroscopy and imaging was possible due to focusing X-ray optics which is effective only at the soft X-ray energy range. Similar improvement in sensitivity of polarisation measurement at soft X-ray range is expected in near future with the advent of GEM based photoelectric polarimeters. However, at energies  $>10$  keV, even spectroscopic and imaging sensitivities of X-ray detector are limited due to lack of focusing optics. Thus hard X-ray polarimetry so far has been largely unexplored area. On the other hand, typically the polarisation degree is expected to increase at higher energies as the radiation from non-thermal processes is dominant fraction. So polarisation measurement in hard X-ray can yield significant insights into such processes. With the recent availability of hard X-ray optics (e.g. with upcoming NuSTAR, Astro-H missions) which can focus X-rays from 5 KeV to 80 KeV, sensitivity of X-ray detectors in hard X-ray range is expected to improve significantly. In this context we explore feasibility

---

T. Chattopadhyay (✉) · S. V. Vadawale  
Physical Research Laboratory, Ahmedabad, Gujarat, India  
e-mail: tanmoy@prl.res.in

J. Pendharkar  
Indian Institute of Science Education and Research (IISER) Pune, Pune, India

*Present Address:*  
J. Pendharkar  
Indian Institute of Tropical Meteorology, Pune, India

of a focal plane hard X-ray polarimeter based on Compton scattering having a thin plastic scatterer surrounded by cylindrical array scintillator detectors. We have carried out detailed Geant4 simulation to estimate the modulation factor for 100 % polarized beam as well as polarimetric efficiency of this configuration. We have also validated these results with a semi-analytical approach. Here we present the initial results of polarisation sensitivities of such focal plane Compton polarimeter coupled with the reflection efficiency of present era hard X-ray optics.

**Keywords** Hard X-ray polarimetry · X-ray instrumentation · Compton polarimetry · X-ray detectors

## 1 Introduction

Since the birth of X-ray astronomy in 1960s, X-ray Polarisation has witnessed almost three decade void while photometry, spectroscopy and imaging have met with significant advancement. The only successful measurement of polarisation in X-ray astronomy dates to 1976 when an X-ray polarimeter onboard OSO-8 mission, measured  $\sim 19\%$  polarisation at 2.6 KeV and 5.2 KeV for the Crab nebula [37]. There were attempts to measure X-ray polarisation, with same polarimeter as well as few other space-born and balloon-born experiments [7, 9, 13, 26, 31] but these could yield only upper-limits at best, due to low sensitivity of these measurements. After these initial efforts, no real experiments to measure X-ray polarisation from celestial X-ray sources were carried out for more than three decades. Though there were some attempts to design and build the X-ray polarimeters (e.g. [1, 33]) and few concept proposals for space missions (e.g. XPE, [4]; PLEXAS, [23]), only one instrument (SXP, [17]) was actually selected for flight on-board Russian mission Spectrum X-Gamma, but unfortunately this mission could not be materialized. This lack of X-ray polarisation measurement experiments was mainly due to very low sensitivity of polarimetry compared to say, spectroscopy, imaging or timing; which results due to extremely photon hungry nature of the X-ray polarimetry.

However, importance of X-ray polarisation measurement has been well known as these measurements provide two independent parameters, i.e. degree and angle of polarisation characterizing the incoming radiation from any X-ray source. These parameters can provide unique opportunity to study the behavior of matter and radiation under extreme magnetic fields and extreme gravitational fields [22, 32]. Importance of the X-ray polarimetry can be understood from the fact that there are many efforts to recover polarimetric information from the existing data obtained by existing detectors [2, 6, 20]. However, since these detectors are not designed or optimized for polarimetric observations, such results remain inconclusive [15, 29, 38].

With recent technological developments in detector technology, attempts are being made by several groups across the globe to develop detectors specifically designed for X-ray polarimetric observations. Particularly, the

development of X-ray polarimeter based on principle of photo-electron tracking as focal plane detector is highly promising and the upcoming GEMS mission [14], based on this type of X-ray polarimeter, is expected to provide orders of magnitude improvement in X-ray polarimetric sensitivity. However, this improvement will be at soft X-ray energies below 10 keV due to very low efficiency of these detectors at higher energies.<sup>1</sup> For measurement of X-ray polarisation at energies above 10 keV it is necessary to employ polarimeters based on Rayleigh/Compton scattering principle [21, 28]. So far scattering based X-ray polarimeters have mostly been considered as collimated detectors operating in hard X-rays/soft gamma-rays, where the Compton scattering based polarimeter has reasonable sensitivity because of their extremely low background. However, with the availability of hard X-ray optics [11, 19] it is also possible to consider the Compton scattering based X-ray polarimeter as a focal plane detector.

Here we investigate a possible implementation of a Compton scattering based X-ray polarimeter and estimate its sensitivity when coupled with NuSTAR type of hard X-ray optics. This work is an offshoot of our earlier work [35] on X-ray polarimeter based on Rayleigh scattering (POLIX mission, [28]) in India which is under active consideration by Indian Space Research Organization (ISRO). As a related experiment in X-ray polarimetry, we are contemplating the proposed configuration (or an alternative configuration where both spectroscopy and polarimetry can be attempted) as a hard X-ray focal plane detector to be proposed to ISRO. The main idea here is to estimate the sensitivity of the focal plane Compton polarimeter considering the collecting area of NuSTAR as a benchmark. Though, consideration has been given to the realization feasibility of the experiment while designing the geometric configuration, the main objective is not to simulate the actual experiment but rather to estimate the sensitivity of the technique. The geometry we have considered is the most optimum geometry for a focal plane Compton polarimeter and thus the sensitivity results presented here are the best possible results one can achieve with the assumed collecting area. In other words, the only other way to increase sensitivity of a Compton polarimeter would be to increase collecting area. Having these sensitivity results as a benchmark would be useful for quantitative comparison of sensitivity of any other configuration of a Compton polarimeter e.g. using different scatterer for additional spectroscopic sensitivity (which is under consideration in our group). Any such deviation from the proposed ‘almost ideal’ configuration would compromise polarimetric sensitivity but this would have to be weighed against additional advantage. Therefore it is important to know the best possible sensitivity for a Compton polarimeter with given collecting area, which is presented here. In the next section we briefly outline the scientific basis for hard

---

<sup>1</sup> According to recent news GEMS mission has been cancelled.

X-ray polarimetry followed by discussion on basic principles of the Compton polarimetry. In Section 4 we discuss the proposed experimental configuration and the simulations with Geant4. Section 5 discusses the validation of the simulated modulation factor and efficiency with semi-analytical calculations. Finally we conclude with discussion on our estimation of sensitivity of a Compton X-ray polarimeter as a focal plane detector.

## 2 Scientific rationale for hard X-ray polarimetry

The X-ray emission in hard X-ray range is typically dominated by non-thermal processes and it is generally accepted that non-thermal processes provide higher degree of polarisation. Thus, in general higher degree of polarisation from X-ray sources is expected at higher energies. Krawczynski et al. [18] have extensively discussed the scientific importance of hard X-ray polarimetry, so here we provide only a brief outline of various classes of X-ray sources for which X-ray polarimetric observations can provide significant insights.

*Binary black hole systems* For binary black holes, at lower energy the flux is dominated by the thermal radiation, which may be polarised via Thomson scattering in the disk atmosphere. If the GR effect is included, the photons move in curved space time and this causes the polarisation fraction to decrease [3]. This effect is dominant for the photons emitted closer to the black hole, for high spin of black hole. Since closer to the black hole temperature of the disk is higher, GR effect is large for high energy and small for low energy flux. This causes the polarisation to be energy dependent. At lower energies ( $E \leq 0.1$  KeV) the degree of polarisation is almost same as that for flat space time, but with the increase in energy polarisation degree decreases. Polarimetric data therefore can constrain parameters like black hole spin, disk inclination.

However at energies greater than 10 KeV, the flux is dominated by the coronal emission. Polarimetry in low hard state can give vital information about the corona structure. Schnittman and Krolik [30] investigated the polarimetric results for various corona geometries. For a homogeneous sandwich corona, at higher inclination the photons move through the disk and are vertically polarised with respect to disk plane. While moving parallel to the disk, they are multiple inverse Compton scattered and boosted upto very high energies. This causes the energy dependent polarisation. At 100 KeV, the expected degree of polarisation is about 10 % at high inclination, for lower inclination, the value decreases. On the other hand for an inhomogeneous clumpy corona, the polarisation decreases to 3–4 % for the same energy, because the photons after being inverse Compton scattered multiple times in one spherical clumpy corona, emerge in all directions, consequently net polarisation decreases. For a simple spherical corona geometry, the expected polarisation fraction is about 4 % at 100 KeV but almost independent of the inclination because of the

spherical symmetry. Therefore the polarisation in low high state can tell a lot about the coronal geometry.

*Blazars* Hard X-ray polarimetry is believed to give information on emission mechanisms in AGN jets. For low energy peaked blazars, the low energy peak occurs at optical regime and high energy peak around MeV. Synchrotron Self Compton model (SSC model) tells that low energy peak is due to synchrotron radiation of the relativistic electrons and high energy peak is due to the inverse Compton scattering of the synchrotron photons off the relativistic electrons itself. Polarisation fraction for synchrotron radiation is higher ( $>60\%$ , for uniform magnetic field) compared to the SSC radiation ( $>30\%$ ) for a particular spectral index of the electron energy distribution and they vary in same manner with the spectral index. However in External Compton model where it is believed that for high energy peak the seed photons are the accretion disk photons or the emission from broad line region or from dusty molecular torus etc. instead of the synchrotron photons the polarisation fraction is below  $5\%$  [24]. Multiwavelength polarimetric observations can test these two models.

For high energy peaked blazars low energy flux peaks in X-ray band whereas the high energy peak occurs in GeV to TeV range. Polarisation measurement of Synchrotron X-ray radiation can indicate the structure of the magnetic field close to the base of jet. High degree of polarisation close to the theoretical values will lead to the presence of uniform magnetic field. On the other hand presence of swing in polarisation will lead to the presence of helical magnetic field in the jet [18]. Therefore broadband polarisation measurement can give vital information about the magnetic field structure in the jet.

*Gamma ray bursts* Origin of magnetic field in GRBs is a debatable issue till now. Both prompt and afterglow emission polarimetry can draw an end to this mystery. The afterglow (appears in X-ray, optical, IR and radio wavebands successively) is believed to be synchrotron radiation from relativistic electrons gyrating in the magnetic field. In standard fireball afterglow model the magnetic field is generated in the shock front and is random. So a small polarisation fraction is expected. Temporal variation of polarisation fraction is connected to the evolution of afterglow phase with maximum polarisation found near the jet break associated with a  $90^\circ$  flip in polarisation angle. Another model, where the outflow is believed to be poynting flux dominated, tells that magnetic field is coherent in large scale and therefore a large degree of polarisation is expected [8]. However the polarisation angle remains constant with time in prompt and afterglow emission and evolution of polarisation fraction is not related to the jet break.

*Neutron stars* X-ray polarimetry can lead us to a better understanding in pulsars, accreting pulsars, magnetars and the QED effects in strong magnetic fields. The details of emissions and emission sites for pulsars have been a subject of debate. The models like polar cap model, outer gap describing different emission sites, correspond to very high polarisation fraction. However both

the models predict quite distinct phase dependent polarisation properties [36]. Phase resolved polarimetry can test the models and help in understanding the emission sites and emission mechanisms. Via X-ray polarimetry, it is also possible to observationally verify the QED effect—vacuum birefringence that arises due to presence of very strong magnetic field. It may give rise to energy dependent polarisation signals in X-rays.

In case of magnetars the magnetic is extremely high ( $10^{14-15}$  G). Radiation emitted in such strong field should be highly polarised. Magnetar's persistent emission is faint in soft X-ray; however, there is a bright hard X-ray tail (20–100 KeV). This range is promising for hard X-ray polarimetry as it will be helpful in understanding the nature of magnetars and the physical processes in extremely strong magnetic fields.

Many accretion-powered pulsars have been found to exhibit cyclotron features in energy range 15–50 KeV. Near cyclotron resonance the polarisation fraction is expected to oscillate with pulse phase. Phase resolved polarisation near cyclotron resonance energies can be used to determine the beam shape of pulsar; for example for pencil beam the oscillations in polarisation fraction are expected to be out of phase with pulse phase, whereas for a fan beam, the opposite case is expected [25]. It will in turn help in understanding the accretion flow to the magnetic poles of the pulsars.

### 3 Compton X-ray polarimetry

The three basic techniques to extract polarisation information of sources are Bragg reflection, Compton scattering and photoelectron imaging. Bragg reflection, despite of achieving high modulation factor, work only at discrete energies which results in low sensitivity. Photoelectron tracking polarimeters (GPD, TPC) are sensitive but can operate mostly in soft X-rays. Polarimeters based on Compton scattering work in hard X-ray with broad energy response. One of the major advantages for Compton polarimeters is very low background compared to the Thomson based polarimeters.

In Compton scattering, the photon is scattered off an electron and imparts a small energy to the electron. The differential cross-section for Compton scattering of a polarized X-ray beam is given by Klein-Nishina formula,

$$\frac{d\sigma}{d\Omega} = \frac{r_0^2}{2} \left( \frac{\nu'}{\nu_0} \right)^2 \left( \frac{\nu'}{\nu_0} + \frac{\nu_0}{\nu'} - 2(\sin\theta)^2(\cos\eta)^2 \right) \quad (1)$$

Where  $\nu_0$ , and  $\nu'$  and energies of incident and scattered photons respectively, given by,

$$\frac{\nu'}{\nu_0} = \frac{1}{1 + \frac{h\nu_0}{mc^2}(1 - \cos\theta)} \quad (2)$$

and  $r_0$  is the classical electron radius,  $m$  is the mass of electron,  $\theta$  is the polar scattering angle, and  $\eta$  is the azimuthal scattering angle i.e. the angle between

the electric vector of the incident photon and the scattering plane as shown in the Fig. 1.

The  $\cos^2\eta$  distribution of scattered photons can be fit by the following function,

$$C(\varphi) = A \cos(2(\varphi - \varphi_0 + \pi/2)) + B \tag{3}$$

Where,  $C(\varphi)$  is the number of events or counts at azimuthal angle  $\varphi$ ,  $\varphi_0$  is the polarisation angle, A, B are constants used for fit. Values of A, B, and  $\varphi_0$  are found from fitting.

This modulation pattern gives the information about the polarisation of the beam. Higher the degree of polarisation, higher will be the modulation of the curve. Modulation factor ( $\mu$ ) is defined as

$$\mu = \frac{C_{\max} - C_{\min}}{C_{\max} + C_{\min}} = \frac{A}{B} \tag{4}$$

The degree of polarisation of the source is defined as

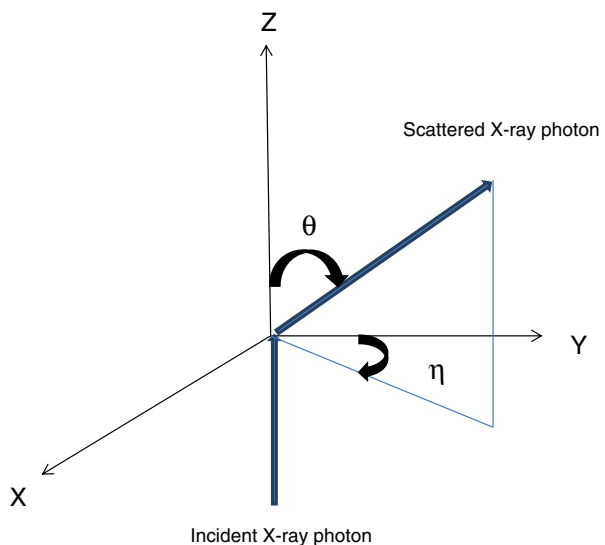
$$P = \frac{\mu}{\mu_{100}} \tag{5}$$

Where  $\mu_{100}$  is the modulation factor for 100 % polarized beam which is calculated using simulation and P is the degree of polarisation of the incident beam.

Sensitivity of the polarisation measurement is given by minimum detectable polarisation (MDP)

$$MDP(\%) = \frac{n_\sigma}{\mu_{100}R_{\text{src}}} \sqrt{\frac{2(R_{\text{src}} + R_{\text{bkg}})}{T}} \tag{6}$$

**Fig. 1** Compton scattering in spherical polar co-ordinates.  $\theta$  is the polar angle and  $\eta$  is the azimuthal angle of scattering. Polarisation is considered to be along Y axis



Where  $n_\sigma$  is the significance level (number of sigma),  $R_{\text{src}}$  is the rate of source counts,  $R_{\text{bkg}}$  is the background count rate,  $T$  is the integration time. To maximize the sensitivity (i.e. to achieve lowest MDP), it is necessary to maximize both modulation factor as well as the overall detection efficiency.

An important feature of the Compton polarimetry is the extremely low background which is achieved due to the requirement of on simultaneous detection of both, the primary Compton scattering event in the scatterer as well as the secondary detection of the scattered photon by surrounding detector. The energy transferred to electron in the scattering event is typically a small fraction of the incident photon energy. Therefore, the lowest energy up to which Compton polarimetry can be extended depends on the lowest energy threshold of the scatterer. The deposited energy is given by

$$E_{\text{dep}} = \frac{(h\nu_0)^2 (1 - \cos\theta)}{mc^2 + h\nu_0 (1 - \cos\theta)} \quad (7)$$

Figure 2 shows that deposited photon energy is a strong function of scattering angle. The deposited energy does not depend on the scatterer material. To maximize sensitivity it is important to increase the source counts which can be

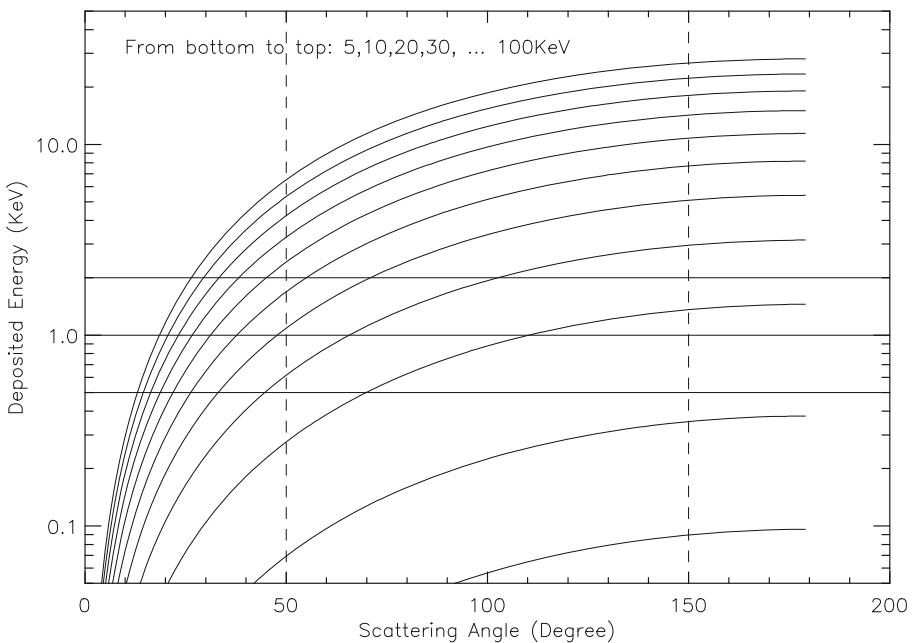


**Fig. 2** Recoil energy of photon as function of scattering angle and incident photon energy. The curves from bottom to top are showing the electron energy for 5 KeV, 10 KeV, 20 KeV... 100 KeV respectively



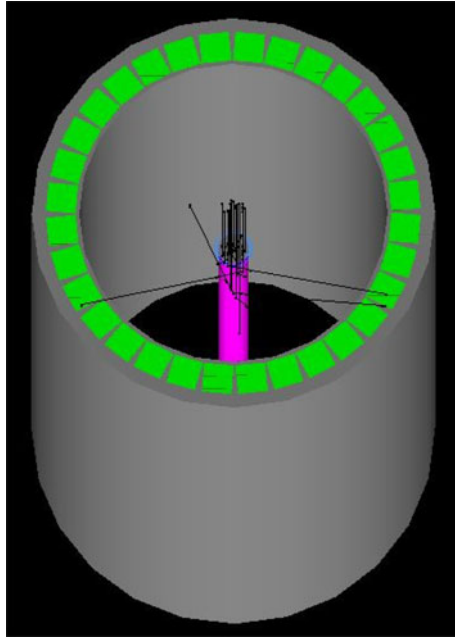
implemented in two ways: one by lowering down the threshold in scatterer and second by expanding the scattering angle range which depends on the scattering geometry. For example assuming scattering angle range between  $50^{\circ}$ – $150^{\circ}$  we see from Fig. 2 that 2 KeV threshold will allow lowest energy cut off to be about 25 KeV, whereas 1 KeV threshold sets the cut off at about 18 KeV; however for 0.5 KeV threshold the lower limit goes down further to 12 KeV. Therefore sensitivity of instrument significantly depends on scattering geometry and energy threshold in scatterer.

#### 4 Proposed detector configuration

As discussed in the previous section, it is necessary to maximize both the modulation factor and the detection efficiency in order to maximize the polarimetric sensitivity. These two parameters are influenced by the type and shape of the scattering element used and must either be measured experimentally or must be determined by means of simulations [35]. The scattering element to be used must be made up of lowest possible  $Z$  material to obtain high efficiency (because the cross-section of the competing photoelectric interaction is proportional to  $Z^5$ ) and it must be designed such that the incident photon sees a larger depth while passing through the volume (to have a significant probability for Compton interaction) and the scattered photon sees a smaller depth in the direction perpendicular to the direction of the incident photon (to minimize multiple interactions within the scattering volume itself). A narrow tube scatterer surrounded by a cylindrical array of detectors would satisfy the above criteria but for its small collecting area.

Here we consider a Compton polarimeter based on this configuration as a focal plane detector for a hard X-ray optics. For the purpose of present simulations, we assume optics effective area similar to that of upcoming NuSTAR optics. The configuration has a low  $Z$  thin scatterer (plastic scintillator) surrounded by cylindrical array of 32 CsI scintillators to record the azimuthal dependence of scattered X-ray photons. The plastic scintillator is used because of its low  $Z$  constituents (C and H) so that the photoelectric absorption is relatively low compared to Compton interaction probability. CsI has very high efficiency to photoelectrically absorb the scattered photons. The plastic scatterer is in cylindrical form of radius 5 mm and length 100 mm. Dimension of the absorbers is 5 mm  $\times$  5 mm  $\times$  150 mm each with total 32 elements in cylindrical array. The modeled configuration is shown in Fig. 3 and also include, additional housing structures (assumed to be made up of thin Al) as would be required for a real detector. This configuration is very close to the ideal Compton polarimeter with very thin active scatterer (to scatter the incident photons) surrounded by a cylindrical detector (to detect scattered photons) and thus expected to have the best possible sensitivity to measure polarisation of the incident X-rays. The exact specifications for the configuration are given in Table 1.

**Fig. 3** View of scattering geometry from the top. The *pink colour cylindrical bar* refers to the plastic scatterer (5 mm diameter and 100 mm length) and the *green bars* are the surrounding 32 CsI scintillators (5 mm  $\times$  5 mm  $\times$  150 mm). The gaps between the scintillators are also seen, these are filled with 0.2 mm Al



#### 4.1 Comparison with other contemporary hard x-ray polarimeters

Many groups worldwide are working for development of Compton hard X-ray polarimeter and some of them are likely to have actual testing/measurement with balloon-born experiment e.g. X-Calibur [10], POLAR [27], PoGOLite [16] etc. Among these, POLAR is an open GRB detector and hence cannot be directly comparable. The PoGOLite is a large area, collimated detector. This type of non-focusing detector, due to much larger detector area, is susceptible

**Table 1** Exact dimensions of the scattering geometries implemented in the application code

Scatterer	
Shape and material	Cylindrical, plastic
Height	100 mm
Diameter	5 mm
Scattering cover	Al with diameter 5 mm and height 5 mm
Absorber	
Shape and material	Cylindrical array of 32 CsI scintillators
Dimension	5 mm $\times$ 5 mm $\times$ 150 mm
Dead space between scintillators	Al with 0.2 mm width
Distance between center of scatterer and front of scintillator	26.5 mm
Thickness of Al cylinder in between scatterer and absorbers	0.5 mm

to large background which severely limits the polarimetric sensitivity and hence it is not expected to match sensitivities of a small sized detector at the focal plane of focussing optics proposed here. X-Calibur is a hard X-ray focal plane Compton polarimeter, whose configuration is conceptually identical to the one proposed here. It consists of a thin scintillator rod surrounded by  $2.5 \text{ mm} \times 2.5 \text{ mm}$  pixelated CZT detectors from four sides. Thus the only difference between the two configurations is that the surrounding detector is square rather than cylindrical as proposed here. However, the square surrounding detector has inherent preferred plane for the azimuthal distribution and thus is likely to introduce artificial modulation when the polarisation direction of the incident X-rays has a particular alignment with respect to the detector. Further, this would typically result in different modulation factors for the cases when incident polarisation plane is parallel to the detector plane or is at  $45^\circ$ . This limitation can be overcome by rotating the polarimeter with respect to the optical axis, however, this requirement of rotation adds additional complication in the realization of the instrument. On the other hand, the cylindrical detector proposed here can avoid this additional requirement. Also due to the intrinsic symmetry, it is expected to have better and stable modulation factor without any preference to polarisation direction of incident X-rays. The pixelated CZT detectors proposed for X-Calibur will have two-dimensional position sensitivity, however, position sensitivity along the length of the plastic scatterer cannot be used to determine the polar scattering angle because exact interaction position in the plastic scatterer cannot be determined. Thus two dimensional position sensitivity of CZT detector only adds additional complexity in electronics in terms of much larger number of readout pixels which can be avoided by simple cylindrical array of scintillators as proposed here. CZT detectors are expected to have better energy resolution; however, again energy resolution of the surrounding detector is not very critical because of very poor energy resolution of the central plastic scatterer in the first place. Thus we think that the proposed configuration is better alternative in terms of feasibility.

## 4.2 Simulation and data analysis

We use Geant4 toolkit [5] to estimate the modulation factor for 100 % polarised beam and efficiency of the instrument. Since we are mainly concerned with interaction of polarized X-ray photons up to energy of  $\sim 100 \text{ keV}$ , we employ the low-energy electromagnetic process. Specifically we use *G4LowEnPolarizedPhotoElectric*, *G4LowEnPolarizedRayleigh*, *G4LowEnPolarizedCompton*, *G4LowEnBremss* and *G4LowEnIonization*. For each of the energies, we carry out simulation for 1000000 photons incident on the scatterer and store the output for each photon detected in the CsI scintillators. A valid event should be defined as one Compton scattering in scatterer and photoabsorption of that scattered photon in absorber. However in real life there is no way to recognize events involving multiple scattering

in scatterer and events where photons suffer scattering in Al cylinder before being absorbed in absorber. Therefore only those events which satisfy the energy cuts in plastic and absorber and simultaneity between them have been declared valid and analysed further. Since it is a focal plane instrument, the photons are made to be incident within a very small perpendicular area of radius 2 mm in the scatterer. The output of each simulation run is stored in the form of event list. It should be noted that, though the event list has much more information, for further analysis, which is carried out separately using IDL, we consider only the information which would be available in the real detector such as deposited energy and CsI crystal number.

Each event line contains the location of interaction in the plastic scatterer and the surrounding CsI scintillators. There are both Compton and Rayleigh scattering events (at lower energies) in the scatterer. We have to ignore the Rayleigh events and consider only the Compton events. The exact location of photon interaction in each scintillator is not possible. In the current design, there are 32 CsI scintillators surrounding the plastic scintillator; thus 32 bins for the azimuthal scattering angle. At each energy simulation code is run for 1 million photons. In Section 3 we discussed that sensitivity of instrument increases if we decrease the threshold in scatterer. We have assumed energy threshold of 1 KeV and 2 KeV. With this assumption first the azimuthal scattering angle is estimated for every valid event. Fitting the histograms of

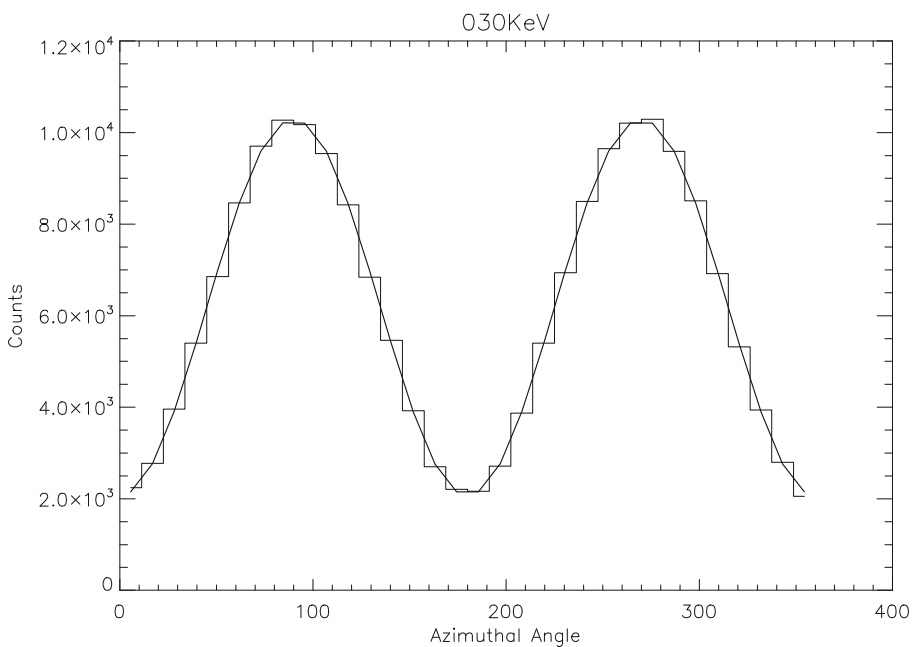


**Fig. 4** Azimuthal distribution of scattered photons at 30 KeV

the azimuthal scattering angles, the modulation factors and polarisation angles are calculated for each of the energies. Figure 4 shows one of such modulation curves at 30 KeV. This particular plot is for 1 KeV energy threshold. Efficiency at each energy is calculated by summing over all the valid Compton events and then dividing it by total incident photons which in our case is 1 million. Estimated modulation factor, efficiency and figure of merit of the polarimeter have been shown in Fig. 6 as discrete points. Black and red are used to denote 1 KeV and 2 KeV threshold respectively. Modulation factor is low at lower energies; since the photons scatter at angles greater than  $90^\circ$ . As energy increases, value of modulation factor increases as now more and more photons are scattered at  $90^\circ$  and reaches maximum. Then the curve almost flattens at higher energies. Efficiency of the polarimeter increases with the energy as expected. Figure of merit is defined as modulation factor multiplied by square root of the efficiency and is inversely proportional to the minimum detectable polarisation if we neglect the source characteristics, time of observation etc.

## 5 Semi-analytic calculation of modulation factor and efficiency

Here we present a semi-analytical treatment to evaluate modulation factors and efficiencies at different energies for the scattering geometry to compare the results with the simulation results to see whether both the results are consistent or not. Advantage of this semi-analytic formulation is that it can be used for quick checking of some geometric variation of the configuration such as length of scatterer, diameter of the surrounding detector, length of the surrounding detector without running full simulation. Thus multiple simulation runs can be avoided for minor changes of the geometrical configurations.

We have divided the scatterer into large number of segments (S). Idea is to calculate  $C_{\max}$  and  $C_{\min}$  in each segment starting from top to bottom and ultimately add them individually to calculate modulation factor. We also considered the transmission probability of the photons from one segment to another in the scatterer which is  $\exp\left(-\mu_t \rho \frac{10}{S}\right)$ . First step is to calculate the total number of photons scattered at polar angle  $\theta$  by the scatterer in each segment for azimuthal angle  $\varphi = \pi/2$  and  $\varphi = 0$  separately.

$$C_{\max}(i, \theta) = N \exp\left(-\mu_t \rho i \frac{10}{S}\right) \left(\frac{\mu_c}{\mu_t}\right) \left(1 - \exp\left(-\mu_t \rho \frac{10}{S}\right)\right) \times \left(\frac{\left(\frac{d\sigma}{d\Omega}\right)_{\varphi=\pi/2} \sin\theta \, d\theta \, d\varphi}{\sigma_t}\right) \quad (8)$$

$$C_{\min}(i, \theta) = N \exp\left(-\mu_t \rho i \frac{10}{S}\right) \left(\frac{\mu_c}{\mu_t}\right) \left(1 - \exp\left(-\mu_t \rho \frac{10}{S}\right)\right) \times \left(\frac{\left(\frac{d\sigma}{d\Omega}\right)_{\varphi=0} \sin\theta \, d\theta \, d\varphi}{\sigma_t}\right) \quad (9)$$

Where,  $i$  signifies each slice and goes from 0 to  $(S-1)$ ,  $N$  is number of incident photons,  $\mu_c$  is the mass absorption coefficient of Compton scattering for plastic in  $\text{cm}^2/\text{gm}$ . unit at energy  $E$ ,  $\mu_t$  is the mass absorption coefficient of total interaction for plastic in  $\text{cm}^2/\text{gm}$ . unit at energy  $E$ ,  $\rho$  is the density of plastic in  $\text{gm}/\text{cc}$  unit.  $\frac{10}{S}$  is the thickness of each segment.  $\sigma_t$  is the total Compton scattering cross-section i.e.

$$\sigma_t = \int_0^\pi \frac{r_0^2}{2} \left(\frac{\nu'}{\nu_0}\right)^2 \left(\frac{\nu'}{\nu_0} + \frac{\nu_0}{\nu'} - (\sin\theta)^2\right) 2\pi \sin\theta \, d\theta \quad (10)$$

The ratio of two cross-sections (1) and (10) gives the fraction of photons scattered at angle  $\theta$ .

Since only those photons which are scattered at a particular angle range will be absorbed by the CsI scintillators, so the next step is to integrate the equation over the  $\theta$  range covered by the surrounding scintillators for each segment. This angle range ( $\theta_{\min}$  to  $\theta_{\max}$ ) depends on the geometry and energy deposition during scattering in plastic scintillator and the segment from where scattering takes place. Here we assume 100 % detection efficiency of the CsI detectors. For each slice,  $\theta_{\min}$  and  $\theta_{\max}$  are to be calculated properly (see Fig. 5). From Figure we see

$$\theta_{\max} = \sin^{-1} \frac{x + 5}{\sqrt{(x + 5)^2 + (2.65 + 0.5)^2}}$$

$$\theta_{\min} = \sin^{-1} \frac{2.65 + 0.5}{\sqrt{(10 - x)^2 + (2.65 + 0.5)^2}}$$

For high energy photons the scattering mainly takes place in the forward direction. The minimum scattering angle depends on the threshold energy in the scatterer and is equal to  $\cos^{-1}\left(1 - \frac{E_{\text{thres}} m_e c^2}{E(E - E_{\text{thres}})}\right)$  where  $E_{\text{thres}}$  is the energy threshold in scatterer and  $E$  is energy of the incident photons. To make sure that only those photons scattered towards the CsI scintillators are counted, we have to take either Sin or Cos whichever is maximum as lower limit of

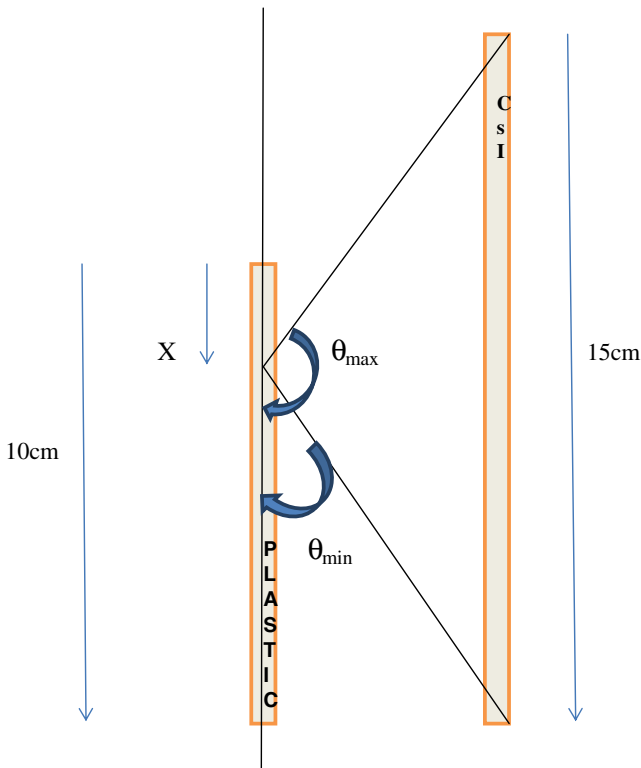


**Fig. 5** View of scattering geometry.  $\theta_{\min}$  is the minimum scattering angle and  $\theta_{\max}$  is the maximum angle of scattering

integration. In the last step the contributions from all the segments are summed over and we get

$$C_{\max} = \sum_{i=0}^{i=S-1} N \exp\left(-\mu_t \rho_i \frac{10}{S}\right) \left(\frac{\mu_c}{\mu_t}\right) \left(1 - \exp\left(-\mu_t \rho \frac{10}{S}\right)\right) \times \left(\frac{\int_{\theta_{\min}}^{\theta_{\max}} \left(\frac{d\sigma}{d\Omega}\right)_{\varphi=\pi/2} \text{Sin}\theta \, d\theta \, d\varphi}{\sigma_t}\right) \tag{11}$$

$$C_{\min} = \sum_{i=0}^{i=S-1} N \exp\left(-\mu_t \rho_i \frac{10}{S}\right) \left(\frac{\mu_c}{\mu_t}\right) \left(1 - \exp\left(-\mu_t \rho \frac{10}{S}\right)\right) \times \left(\frac{\int_{\theta_{\min}}^{\theta_{\max}} \left(\frac{d\sigma}{d\Omega}\right)_{\varphi=0} \text{Sin}\theta \, d\theta \, d\varphi}{\sigma_t}\right) \tag{12}$$

Modulation factor can be obtained from (11) and (12)

$$\mu(E) = \frac{C_{\max} - C_{\min}}{C_{\max} + C_{\min}} \tag{13}$$

Efficiency calculation is similar. Assuming 100 % efficiency of the CsI detectors in the energy range of operation, we estimate the polarimetric efficiency by calculating the total number of photons scattered by all the segments in the plastic scatterer towards the surrounding CsI scintillators. Using the same approach, the efficiency comes out to be:

$$\begin{aligned} \epsilon = & \sum_{i=0}^{i=S-1} N \exp\left(-\mu_t \rho_i \frac{10}{S}\right) \left(\frac{\mu_c}{\mu_t}\right) \left(1 - \exp\left(-\mu_t \rho \frac{10}{S}\right)\right) \\ & \times \left(\frac{\int_{\theta_{\min}}^{\theta_{\max}} \left(\frac{d\sigma}{d\Omega}\right) 2\pi \sin\theta d\theta}{\sigma_t}\right) \end{aligned} \tag{14}$$

To take care of the dead spaces in between the CsI detectors a factor  $\left(1 - \frac{32 \times 0.02}{2\pi \times 2.65}\right)$  is multiplied with the above equation.

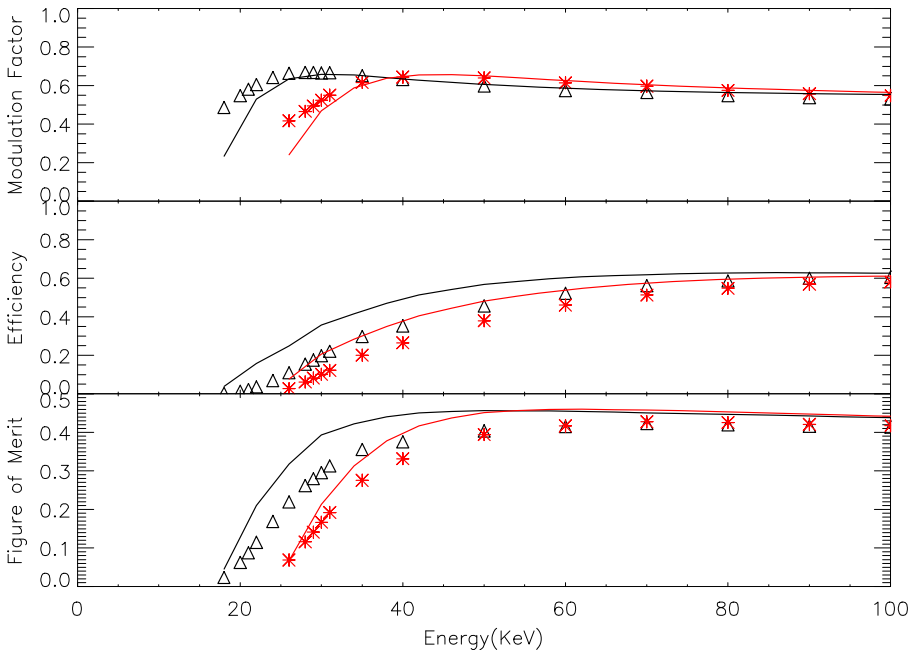


**Fig. 6** Modulation factor, polarimeter efficiency and figure of merit as a function of energy. Black triangles and black solid line represent simulation and analytical results respectively for 1 KeV threshold. Red asterisks and red solid line represent the simulation and analytical results respectively for 2 KeV threshold



Results of these calculations are shown in Fig. 6 as continuous line. It can be seen that the semi-analytical results for modulation factor agree well with the simulation results for most of the energy range, though there is slight discrepancy at lower energies. In case of efficiency, the simulated efficiency is slightly lower than the calculated one. However, it should be noted that in this analytic calculation, we have ignored some of the second order effects such as the multiscattering in surrounding scintillators and the scatterer itself, escape of photons from the CsI detectors, the absorption of scattered photons within the Al in between the scatterer and surrounding scintillators. These factors are not significant for modulation factor, particularly when the number of detected photons is very large. Modulation factor will depend on the angle range mainly, that is why we see good agreement in the results of analytical and simulation results. However these factors are critical for efficiency calculation and as a result analytical model gives slightly higher values of efficiency.

## 6 Sensitivity estimation

Sensitivity of polarimeter (see (6)) depends on energy integrated modulation factor in the energy range of operation for 100 % polarised beam, exposure time, background and rate at which source photons are detected by the instrument which in turn depends on efficiency of polarimeter, source intensity and effective area of the mirror used to focus the X-rays. For MDP calculation we have used the NuSTAR optics effective area [12]. NuSTAR can focus photons from 5 KeV to 80 KeV. If the threshold is 2 KeV, polarimeter can start working from 26 KeV whereas for 1 KeV threshold lower cut off is 18 KeV. First the average modulation factor is estimated in the working energy range (26 KeV–80 KeV and 18 KeV–80 KeV) which for 1 KeV and 2 KeV threshold is around 60.5 % and 60 % respectively which proves the excellent polarimetric performance of this focal plane polarimeter. Source count rate is calculated as follows

$$R_{\text{src}} = \int_{E_1}^{E_2} A_{\text{eff}}(E) I(E) \varepsilon(E) dE \quad (15)$$

Where  $A_{\text{eff}}(E)$  is the effective area of NuSTAR,  $I(E)$  is the source intensity for Crab like spectrum,  $\varepsilon(E)$  is the polarimeter efficiency at energy  $E$ . Value of  $E_1$  depends on threshold in scatterer and  $E_2$  is 80 KeV as we are considering NuSTAR optics. We have considered 100 ks and 1 Ms exposure for sensitivity estimation. Background calculation is discussed in detail below.

### 6.1 Spurious events calculation

Background for a focal plane Compton polarimeter is generally very small. The only source of spurious events in Compton polarimeters is the chance

coincidence between the random background events in the scatterer and in the absorbers within the coincidence time window. Using Poisson's statistics in the coincidence window one obtains the rate of spurious events due to the chance coincidence,

$$N_{\text{sp}} = (1 - \exp(-N_{\text{Scatterer}}\delta T)) N_{\text{absorber}} \quad (16)$$

Where  $N_{\text{scatterer}}$  ( $= N_1 + N_2$ ) is the sum of rate of random background events in the scatterer ( $N_1$ ) and the cosmic X-ray background rate ( $N_2$ ) in scatterer.  $N_{\text{absorber}}$  is the rate of random instrumental background events in the absorbers. Rate at which the cosmic X-ray photons are detected in the scatterer has been calculated using cosmic X-ray background spectrum [34]. Since the FOV of focal plane detector is very small, this value is very small. The cosmic X-ray photons coming from the sky within the detector field of view may be scattered by the scatterer and absorbed by the absorbers. This may also lead to spurious Compton events ( $N_{\text{sky}}$ ). Therefore the rate of total spurious events in the polarimeter can be written as

$$N_{\text{sp}} = (1 - \exp(-N_{\text{Scatterer}}\delta T)) N_{\text{absorber}} + N_{\text{sky}} \quad (17)$$

Since the value of  $N_{\text{sky}}$  is very small due to narrow FOV, the random particle events will dominate the background. Since the actual instrumental background generally depend on the variety of factors such as spacecraft, orbit, time etc. which cannot be estimated at present, we assumed a range of instrumental background rate from  $0.5 \text{ cnt-cc}^{-1}\text{-s}^{-1}$  as a typical condition and  $5 \text{ cnt-cc}^{-1}\text{-s}^{-1}$  as extreme condition. We calculated the spurious events rates corresponding to these two limiting instrumental background rates keeping the time coincidence window of  $10 \mu\text{s}$ , which is then used for calculating MDP values.

## 7 Results and discussions

With the method discussed in previous section we estimated MDP for different Crab intensities which are shown in Fig. 7. We see for 100 mCrab source the MDP is 0.9% with  $3\sigma$  confidence level with one million seconds of exposure time (black solid lines, asterisks), which qualifies this focal plane polarimeter as a sensitive instrument. However for 100 ks exposure, the sensitivity decreases to 3 %. We have also analysed the simulation data by selecting only valid/ideal Compton events and find that the results are almost identical, which suggests that this configuration is very close to the ideal Compton polarimeter configuration. MDP values have been calculated for random instrumental background rate of  $0.5 \text{ cnt-cc}^{-1}\text{-s}^{-1}$  (thin lines) and in extreme condition of  $5 \text{ cnt-cc}^{-1}\text{-s}^{-1}$  (thick lines); however there is not much change in MDP with

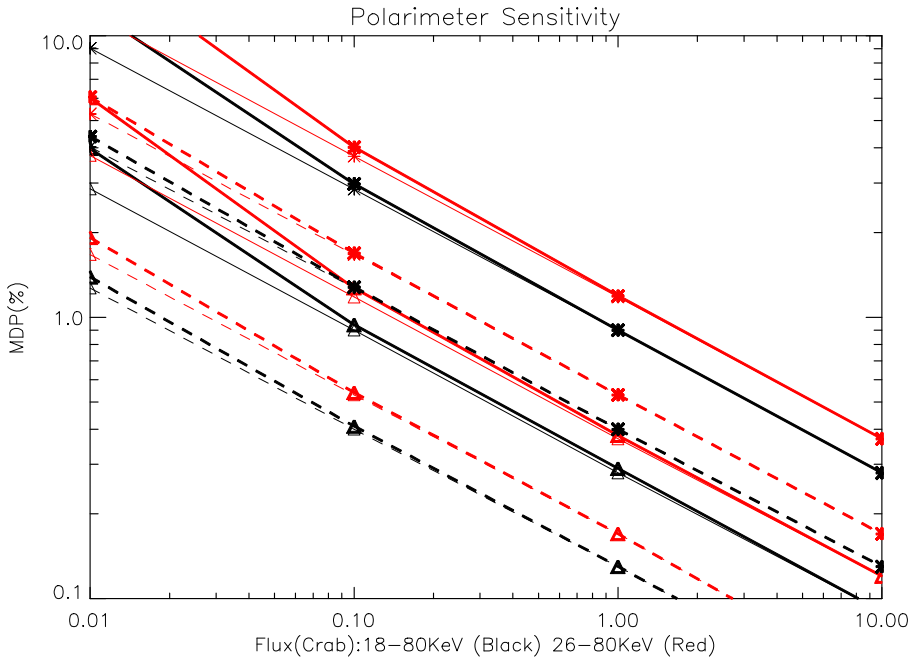


**Fig. 7** MDP as a function of Crab intensity. *Solid lines* represent results for single NuSTAR area. *Dashed lines* refer to 5 times larger NuSTAR area. 1 Ms and 100 ks exposure time are denoted by *triangles* and *asterisks* respectively. The background considered here is  $0.5 \text{ cnt-cc}^{-1}\text{-s}^{-1}$  (*thin lines*) and  $5 \text{ cnt-cc}^{-1}\text{-s}^{-1}$  (*thick lines*)

background beyond 100 mCrab. In Fig. 7 we have shown that sensitivity can be increased significantly using next generation of hard X-ray focusing optics with collecting area 5 times larger than that of NuSTAR area (dashed lines). With this configuration MDP for 100 mCrab decreases to 0.4 % for one million seconds exposure and 1.3 % for 100 ks exposure. Figure 7 clearly suggests that sensitivity of the polarimeter is improved for 1 KeV energy threshold in scatterer instead of 2 KeV. In Fig. 8, we have shown that energy dependent polarisation measurement is possible via this focal plane polarimeter which is very useful to study the X-ray objects. Assuming energy resolution about 10 KeV FWHM, estimated MDP for 100 mCrab and 1Crab have been shown in Figure (triangle and asterisks) for 1 Ms exposure. The dashed lines correspond to the 5 times larger NuSTAR area. The slight difference in sensitivity at lower energies for 1 KeV (black) and 2 KeV (red) threshold is due to higher modulation factor and efficiency for 1 KeV threshold compared to 2 KeV threshold. A particular energy corresponds to almost same amount of flux. As energy increases, modulation factor for 2 KeV threshold exceeds that for 1 keV threshold, however due to low efficiency the MDP values remain almost same.

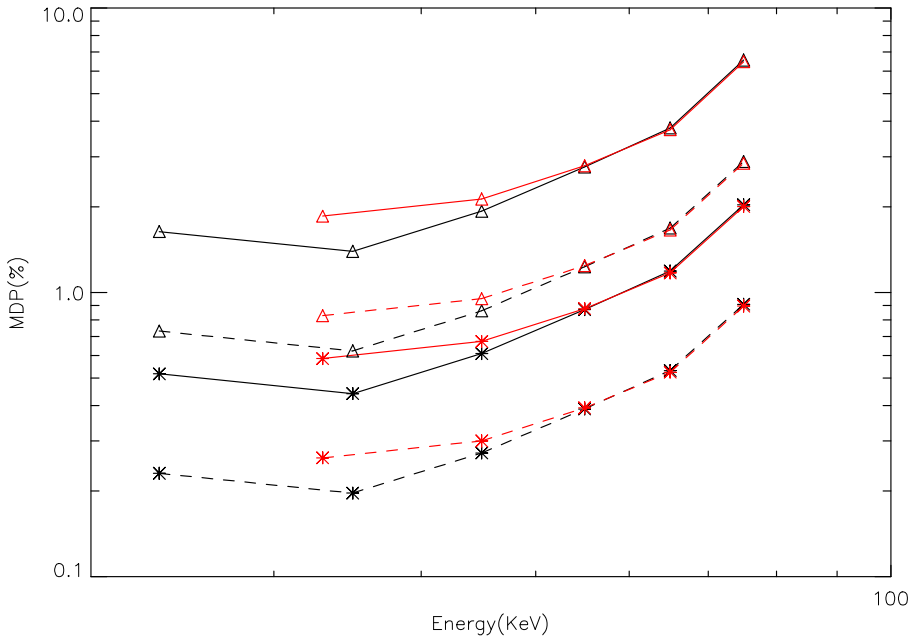


**Fig. 8** Energy dependent MDP of the Compton Polarimeter. *Triangle* and *asterisks* are used to denote 100 mCrab and 1Crab intensity. *Red* and *black* stand for 2 KeV and 1 KeV threshold. *Dashed lines* represent 5 times larger NuSTAR area. The exposure time taken here is 1 Ms and background is  $0.5 \text{ cnt-cc}^{-1}\text{-s}^{-1}$

## 8 Conclusions

Hard X-ray polarimetry is an important tool for understanding various X-ray sources. Here we described a Compton polarimeter as a focal plane detector for a hard X-ray optics. Geant 4 simulations suggest that we can achieve 1 % MDP at 100 mCrab with this instrument with 1 Ms exposure. In Section 2 polarimetric aspects of different sources have been discussed. To measure polarisation from those sources we need this kind of sensitivity. However with next generation of hard X-ray focussing optics we can achieve better sensitivity with this kind of focal plane polarimeter. We are building a prototype of the instrument. As simulation results suggests energy threshold is the key parameter which will decide the sensitivity of the instrument. Therefore it is important to measure the threshold in plastic first and lower it down as much as possible before integrating the whole system to measure sensitivity by shining it with a 100 % polarised beam. The results of the prototype of the instrument will be reported in near future.

**Acknowledgement** We thank anonymous referee for a critical review and very helpful suggestions.

## References

1. Angel, J.R.P., Weisskopf, M.C.: Use of highly reflecting Crystals for spectroscopy and polarimetry in X-ray astronomy. *Astron. J.* **75**, 231–236 (1970)
2. Coburn, W., Boggs, S.E.: Polarisation of the prompt  $\gamma$ -ray emission from the  $\gamma$ -ray burst of 6 December 2002. *Nature* **423**, 415–417 (2003)
3. Dovciak, M., Muleri, F., Goosmann, R.W., Karas, V., Matt, G.: Thermal disc emission from a rotating black hole: x-ray polarization signatures. *MNRAS* **391**, 32–38 (2008)
4. Elsner, R.F., Ramsey, B.D., O'dell, S.L., Sulkanen, M., Tennant, A.F., Weisskopf, M.C., Gunji, S., Minamitani, T., Austin, R.A., Kolodziejczak, J., Swartz, D., Garmire, G., Meszaros, P., Pavlov, G.G.: The x-ray polarimeter experiment (XPE). *Am. Astron. Soc.* **29**, 790 (1997)
5. Geant4 Collaboration, Agostinelli, S., Allison, J., Amako, K., et al.: Geant4—a simulation toolkit. *Nucl. Instrum. Methods Phys. Res. A* **506**, 250–303 (2003)
6. Gotz, D., Laurent, P., Lebrun, F., Daigne, F., Bosnjak, Z.: Variable polarisation measured in the prompt emission of GRB 041219A using IBIS on board INTEGRAL. *ApJL* **695**, L208–L212 (2009)
7. Gowen, R.A., Cooke, B.A., Griffiths, R.E., Ricketts, M.J.: An upper limit to the linear x-ray polarisation of Sco X-1. *MNRAS* **179**, 303–310 (1977)
8. Granot, J., Konigl, A.: Linear polarisation in gamma ray bursts: the case for an ordered magnetic field. *ApJL* **594**, L83–L87 (2003)
9. Griffiths, R.E., Cooke, B.A., Ricketts, M.J.: Observations of the X-ray nova A0620-00 with the Ariel V crystal spectrometer/polarimeter. *MNRAS* **177**, 429–440 (1976)
10. Guo, Q., Garson, A., Beilicke, M., Martin, J., Lee, K., Krawczynski, H.: Design of a hard X-ray polarimeter: X-Calibur. [arXiv:1101.0595](https://arxiv.org/abs/1101.0595)
11. Harrison, F.A., Christensen, F.E., Craig, W., Hailey, C., Baumgartner, W., Chen, C.M.H., Chonko, J., Cook, W.R., Koglin, J., Madsen, K.-K., Pivavoroff, M., Boggs, S., Smith, D.: Development of the HEFT and NuSTAR focusing telescopes. *Exp. Astron.* **20**, 131–137 (2005)
12. Harrison, F.A., et al.: The nuclear spectroscopic telescope array (NuSTAR). In: *Proc. SPIE*, vol. 7732, pp. 77320S–77320S-8 (2010). doi:[10.1117/12.858065](https://doi.org/10.1117/12.858065)
13. Hughes, J.P., Long, K.S., Novick, R.: A search for x-ray polarisation in cosmic x-ray sources. *ApJ* **280**, 255–258 (1984)
14. Jahoda, K.: The gravity and extreme magnetism small explorer. In: *Proc. SPIE*, vol. 7732, pp. 77320W–77320W-11 (2010). doi:[10.1117/12.857439](https://doi.org/10.1117/12.857439)
15. Jourdain, E., Roques, J.P., Malzac, J.: The emission of Cygnus X-1: observations with INTEGRAL SPI from 20 KeV to 2 MeV. *ApJ* **744**, 64–71 (2012)
16. Kamae, T., et al.: PoGO Lite—a high sensitivity balloon-borne soft gamma-ray polarimeter. *Astropart. Phys.* **30**, 72–84 (2008)
17. Kaaret, P.E., Schwartz, J., Soffitta, P., Dwyer, J., Shaw, P.S., Hanany, S., Novick, R., Sunyaev, R., Lapshov, I.Y., Silver, E.H., Ziocck, K.P., Weisskopf, M.C., Elsner, R.F., Ramsey, B.D., Costa, E., Rubini, A., Feroci, M., Piro, L., Manzo, G., Giarrusso, S., Santangelo, A.E., Scarsi, L., Perola, G.C., Massaro, E., Matt, G.: Status of the stellar x-ray polarimeter for the spectrum-x-gamma mission. *Proc. SPIE* **2010**, 22–26 (1994)
18. Krawczynski, H., Garson, A., Guo, Q., Baring, M.G., Ghosh, P., Beilicke, M., Lee, K.: Scientific prospects for hard X-ray polarimetry. *Astropart. Phys.* **34**, 550–603 (2011)
19. Kunieda, H. et al.: Hard X-ray telescope to be onboard ASTRO-H. In: *Proc. SPIE*, vol. 7732, pp. 773214–773214-12 (2010). doi:[10.1117/12.856892](https://doi.org/10.1117/12.856892)
20. Laurent, P., Rodriguez, J., Wilms, J., Bel, M.C., Pottschmidt, K., Grinberg, V.: Polarized gamma-ray emission from the galactic black hole Cygnus X-1. *Science* **332**, 438–439 (2011)
21. Legere, J.S., Bloser, P., Macri, J.R., McConnell, M.L., Narita, T., Ryan, J.M.: Developing a Compton polarimeter to measure polarisation of hard x-rays in the 50–300 KeV range. *Proc. SPIE* **5898**, 413–422 (2005)
22. Lei, F., Dean, A.J., Hills, G.L.: Compton polarimetry in gamma-ray astronomy. *Space Sci. Rev.* **82**, 309–388 (1997)
23. Marshall, H.L., Murray, S.S., Chappell, J.H., Schnopper, H.W., Silver, E.H., Weisskopf, M.C.: Realistic, inexpensive, soft x-ray polarimeter and the potential scientific return. *Proc. SPIE* **4843**, 360–371 (2003)

24. McNamara, A.L., Kuncic, Z., Wu, K.: X-ray polarisation in relativistic jets. *MNRAS* **395**(3), 1507–1514 (2009)
25. Meszaros, P., Novick, R., Szeentgyorgyi, A., Chanan, G.A., Weisskopf, M.C.: Astrophysical implications and observational prospects of x-ray polarimetry. *ApJ* **324**, 1056–1067 (1988)
26. Novick, R., Weisskopf, M.C., Bertherlsdorf, R., Linke, R., Wolff, R.S.: Detection of x-ray polarisation of the Crab Nebula. *ApJL* **174**, L1–L8 (1972)
27. Orsi, S., et al.: POLAR: a space-borne X-ray polarimeter for transient sources. *ASTRA* **7**, 43–47 (2011)
28. Rishin, P.V., Paul, B., Duraiachelvan, R., Marykutty, J., Jincy, D., Cowsik, R.: Development of a Thomson x-ray polarimeter. In: Proc. The Coming of Age of X-ray Polarimetry, pp. 83–87 (2009)
29. Rutledge, R.E., Fox, D.B.: Re-analysis of polarisation in the  $\gamma$ -ray flux of GRB 021206. *MNRAS* **350**, 1288–1300 (2004)
30. Schnittman, J.D., Krolik, J.H. *ApJ*: X-ray polarisation from accreting black holes: coronal emission. *Astrophys. J.* **712**, 908–924 (2010)
31. Silver, E.H., Weisskopf, M.C., Kestenbaum, H.L., Long, K.S., Novick, R., Wolff, R.S.: The first search for x-ray polarisation in the CENTAURUS X-3 and HERCULES X-1. *ApJ* **232**, 248–254 (1979)
32. Soffitta, P.: X-ray polarimetry an ‘almost’ new frontier for X-ray astronomy. In: Italian Physical Society Conference Proceedings Series, vol. 57, pp. 561–573 (1997). ISBN: 8877940964
33. Tsunemi, H., Hayashida, K., Tamura, K., Nomoto, S., Wada, M., Hirano, A., Miyata, E.: Detection of x-ray polarisation with a charge coupled device. *Nucl. Instrum. Methods Phys. Res. A* **321**, 629–631 (1992)
34. Turler, M., Chernyakova, M., Courvoisier, T., Lubinski, P., Neronov, A., Produit, N., Walter, R.: INTEGRAL hard x-ray spectra of the cosmic x-ray background and galactic ridge emission. *Astron. Astrophys.* **512**, 181 (2010)
35. Vadawale, S.V., Paul, B., Pendharkar, J., Naik, S.: Comparative study of different scattering geometries for the proposed Indian x-ray polarisation measurement experiment using geant4. *Nucl. Instrum. Methods Phys. Res. A* **618**, 182–189 (2010)
36. Weisskopf, M.C., Elsner, R.F., Hanna, D., Kapsi, V.M., Odell, S.L., Pavlov, G.G., Ramsey, B.D.: The prospects for X-ray polarimetry and its potential use for understanding neutron stars (2006). [arXiv:astro-ph/0611483](https://arxiv.org/abs/astro-ph/0611483)
37. Weisskopf, M.C., Silver, E.H., Kestenbaum, H.L., Long, K.S., Novick, R.: A precision measurement of the x-ray polarisation of the Crab Nebula without pulsar contamination. *ApJL* **220**, L117–L121 (1978)
38. Wigger, C., Hajdas, W., Arzner, K., Gudel, M., Zehnder, A.: Gamma-ray burst polarisation: limits from RHESSI measurements. *ApJ* **613**, 1088–1100 (2004)